

Finite-difference time-domain simulation of thermal noise in open cavities

Jonathan Andreasen,¹ Hui Cao,^{1,*} Allen Taflove,² Prem Kumar,^{1,2} and Chang-qi Cao³¹*Department of Physics and Astronomy, Northwestern University, Evanston, Illinois 60208-3112, USA*²*Department of Electrical Engineering and Computer Science, Northwestern University, Evanston, Illinois 60208-3112, USA*³*Department of Physics, Peking University, Beijing 100871, China*

(Received 24 September 2007; published 8 February 2008)

A numerical model based on the finite-difference time-domain (FDTD) method is developed to simulate thermal noise in open cavities owing to output coupling. The absorbing boundary of the FDTD grid is treated as a blackbody, whose thermal radiation penetrates the cavity in the grid. The calculated amount of thermal noise in a one-dimensional dielectric cavity recovers the standard result of the quantum Langevin equation in the Markovian regime. Our FDTD simulation also demonstrates that in the non-Markovian regime the buildup of the intracavity noise field depends on the ratio of the cavity photon lifetime to the coherence time of thermal radiation. The advantage of our numerical method is that the thermal noise is introduced in the time domain without prior knowledge of cavity modes.

DOI: [10.1103/PhysRevA.77.023810](https://doi.org/10.1103/PhysRevA.77.023810)

PACS number(s): 42.25.Kb, 05.40.-a, 44.40.+a

I. INTRODUCTION

The finite-difference time-domain (FDTD) method [1] has been extensively used in solving Maxwell's equations for dynamic electromagnetic (EM) fields. The absorbing boundary condition based on the perfectly matched layer (PML) [2] allows the simulation of open systems, e.g., leaky optical cavities, in any dimension. The incorporation of auxiliary differential equations, such as the rate equations for atomic populations [3] and the Maxwell-Bloch equations for the density of states of atoms [4–6], has led to comprehensive studies of light-matter interactions. Although the FDTD method has become a powerful tool in computational electrodynamics, it is applied mostly to classical or semiclassical problems. Recently, quantum fluctuations due to the spontaneous emission of atoms were introduced to the FDTD simulation of microcavity lasers [7]. The light field in an open cavity also experiences quantum fluctuation because of its coupling to external reservoirs. In this paper, we model the quantum noise for the cavity field as a classical noise and incorporate it into the FDTD algorithm.

There are two dissipation mechanisms for the cavity field: (i) Intracavity absorption and (ii) output coupling. In the modal picture, widely used in quantum optical studies, thermal noise is introduced so that the quantum operator of a leaky cavity mode satisfies the commutation relation. Although thermal noise is quantitatively insignificant at optical frequencies, its proper treatment constitutes an essential part of the exact quantum-mechanical theory of lasers. Early laser theory introduces the thermal noise via a heatbath made up of loss oscillators or absorbing atoms [8,9]. It accounts for light absorption inside the cavity. For a laser cavity whose loss only comes from the output coupling, the thermal noise is attributed to the thermal radiation that penetrates the cavity through the coupling [10,11]. Thus the amount of thermal noise depends on the mode decay rate, which must be known in order to solve the Langevin equation for the field operator.

For open complex cavities, e.g., the ones made of random structures, the required information of modes is unknown *a priori*. Thus it is desirable to be able to study the noise of a cavity field without prior knowledge of cavity modes. Additional problems with the modal picture are as follows. (i) If the cavity is very leaky, the significant overlap of modes in frequency makes it difficult to distinguish one mode from another. (ii) In the presence of nonlinearity, strictly speaking, the modes do not exist. In fact, one advantage of the FDTD method is the direct time-domain calculation of EM fields without prior knowledge of modes. The effective modal behavior is an *emergent* property that results from temporal evaluation of the EM fields. We intend to introduce noise to the EM field in a way compatible with the FDTD method, namely, without invoking the modal picture. Our goal is to open a different approach for the study of quantum mechanical aspects of radiation in macroscopic systems with classical electrodynamics simulations. We believe our approach has the potential to permit rigorous theoretical investigations of noise in the area of quantum optics and of open systems such as chaotic open cavities. The dynamics of such systems are, in particular, very difficult to study using the standard frequency domain methods.

In FDTD simulations, it is rather straightforward to introduce noise related to intracavity absorption. A fluctuating electric field can be added as a soft source at every grid point inside the cavity with its rms amplitude proportional to the local absorption coefficient [12,13]. The output coupling, however, is not a local loss. The question is how to introduce thermal noise related to cavity leakage without knowing the leakage rate. In FDTD simulations, light escaping from an open system is absorbed by the absorbing boundary layer (ABL) which acts as the external reservoir. Since it absorbs all impinging fields, the ABL can be modeled as a blackbody. To remain in thermal equilibrium, the blackbody must radiate into the system. The blackbody radiation from the ABL propagates into the cavity and acts as noise to the cavity field. The amount of noise penetrating the cavity depends on the cavity openness or output coupling. We simulate the blackbody radiation from the ABL in the FDTD calculation. Our model is validated in the calculation of field noise in a

*h-cao@northwestern.edu

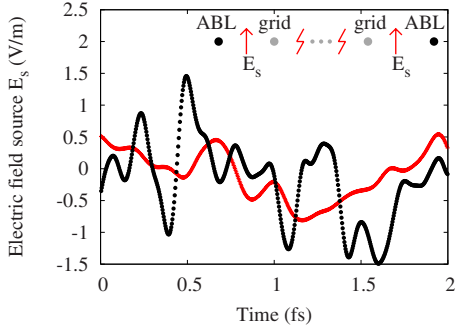


FIG. 1. (Color online) Noise source electric field $E_s(t_j)$ generated for $T=30\,000$ K (black dots) and $T=50\,000$ K (red crosses). The noise correlation time $\tau_c \approx 0.337$ fs for $T=30\,000$ K and $\tau_c \approx 0.203$ fs for $T=50\,000$ K. $\Delta x=1$ nm, $M=2^{21}$, and $\tau_{\text{sim}}=7$ ps. The inset is a schematic showing the noise sources placed next to the grid-ABL interface.

one-dimensional dielectric cavity. In a good cavity whose lifetime τ is much longer than the coherence time of thermal radiation τ_c , the average amount of thermal noise in one cavity mode agrees to the solution of the quantum Langevin equation under the Markovian approximation. In addition to recovering the standard results, our simulations with various values of τ and τ_c illustrate the transition from the Markovian regime to the non-Markovian regime and demonstrate that the buildup of the intracavity noise field depends on the ratio of τ_c to τ . This result is explained qualitatively by interference effect.

The paper is organized as follows. Section II outlines our numerical method. Possible numerical difficulties and problems are discussed. In Sec. III we present the results of the FDTD calculations, including the blackbody radiation in vacuum and noise penetration into a one-dimensional (1D) cavity. The transition from the Markovian regime to the non-Markovian regime is studied. Section IV consists of a discussion and interpretation of the results. An analytical expression is found which offers further insights to the amount of noise inside an open cavity. We end in Sec. V by summarizing all results and including a discussion of future applications for our method.

II. NUMERICAL METHOD

Our numerical model is based on the key insight that the ABL normally used to bound FDTD computational grids is in effect a blackbody which ideally absorbs all incident radiation. To stay in thermal equilibrium with temperature T , the blackbody must radiate into the system. To simulate the blackbody radiation, we surround the grid with a series of noise sources next to the grid-ABL interface. These soft sources radiate EM waves into the grid having spectral properties consistent with blackbody radiation. In this paper, we focus on 1D systems. The 1D grid is discretized with a spatial step Δx and time step Δt . As shown in the inset of Fig. 1, two point sources are placed at the extremities of the grid. Each source generates an electric field E_s at every time step t_j . Examples of the noise source of electric field $E_s(t_j)$ are

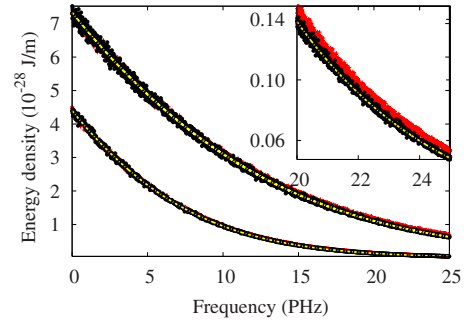


FIG. 2. (Color online) FDTD-calculated energy density of blackbody radiation propagating in 1D vacuum vs frequency ω for temperatures $T=30\,000$ K (lower) and $T=50\,000$ K (upper). The inset shows the energy density for temperature $T=30\,000$ K at higher frequencies. The data are obtained by averaging over 2000 calculations with the resolutions $\Delta x=10$ nm (red crosses) and $\Delta x=1$ nm (black dots). The source spectra $D(\omega, T)$ are also plotted as solid lines on top of the numerical spectra.

shown in Fig. 1. A Fourier transform of the temporal correlation function of the electric field, $\langle E_s(t_1)E_s(t_2) \rangle$, gives the noise spectrum $D(\omega, T)$. If $E_s(t_j)$ is uncorrelated in time, i.e., $\langle E_s(t_1)E_s(t_2) \rangle \propto \delta(t_2-t_1)$, $D(\omega, T)$ is the white-noise spectrum. This is incorrect as $D(\omega, T)$ should be equal to the energy density of the blackbody radiation [14,15], which in one dimension is

$$D(\omega, T) = \frac{\hbar}{\pi c} \left(\frac{\omega}{\exp(\hbar\omega/kT) - 1} \right). \quad (1)$$

$D(\omega, T)$ for two different temperatures is plotted in Fig. 2. For computational convenience, we extend the range of ω from $(0, \infty)$ to $(-\infty, \infty)$. Since the electric field in the FDTD simulation is a real number, $D(-\omega, T)$ must be equal to $D(\omega, T)$ for $\omega > 0$. Therefore, $D(\omega, T) = D(|\omega|, T)$. We normalize $D(\omega, T)$ as

$$D_n(|\omega|, T) = \frac{6\hbar^2}{\pi k^2 T^2} \left(\frac{|\omega|}{\exp(\hbar|\omega|/kT) - 1} \right) \quad (2)$$

so that $\int_{-\infty}^{\infty} D_n(|\omega|, T) d\omega = 2\pi$.

The temporal correlation function for the source electric field is given by

$$\langle E_s(t_1)E_s(t_2) \rangle = \frac{\delta^2}{2\pi} \int_{-\infty}^{\infty} d\omega D_n(|\omega|, T) e^{i\omega(t_2-t_1)}, \quad (3)$$

where δ is the rms amplitude of the noise field whose value is to be determined later. For the thermal noise, the field correlation function is given specifically by

$$\begin{aligned} \langle E_s(t_1)E_s(t_2) \rangle = & \frac{3\delta^2}{\pi^2} [\zeta(2, 1 - i(t_2 - t_1)kT/\hbar) \\ & + \zeta(2, 1 + i(t_2 - t_1)kT/\hbar)], \end{aligned} \quad (4)$$

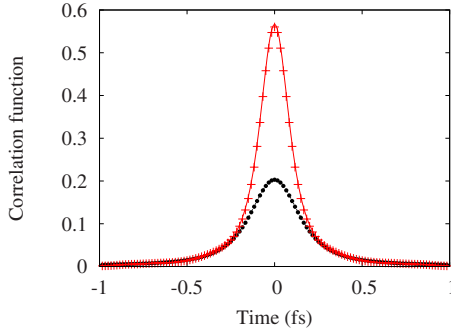


FIG. 3. (Color online) Temporal correlation function, $\langle E_s(t_1)E_s(t_2) \rangle$ vs t_2-t_1 for the noise electric field at $T=30\,000$ K (black circles) and $T=50\,000$ K (red crosses). The noise correlation times are $\tau_c \approx 0.337$ fs for $T=30\,000$ K and $\tau_c \approx 0.203$ fs for $T=50\,000$ K. $\Delta x=1$ nm, $M=2^{21}$, and $\tau_{\text{sim}}=7$ ps. The lines represent $\langle E_s(t_1)E_s(t_2) \rangle$ given by the analytical expression in Eq. (4) for $T=30\,000$ K (black) and $T=50\,000$ K (red). Every fifth data point is taken from the numerical data in order to better show the agreement with the analytical solution.

where the ζ function is given as

$$\zeta(s, a) = \sum_{k=0}^{\infty} (k+a)^{-s}. \quad (5)$$

The temporal correlation function of thermal radiation is plotted in Fig. 3.

We employ a quick and straightforward way of generating random numbers for $E_s(t_j)$ so that Eq. (3) is satisfied. Freilikher *et al.* have developed such a method in the context of creating random surfaces with specific height correlations [16]. The end result takes advantage of the fast Fourier transform (FFT) which we use to generate the source electric field

$$E_s(t_j) = \frac{\delta}{\sqrt{\tau_{\text{sim}}}} \sum_{l=-M}^{M-1} (M_l + iN_l) D_n^{1/2}(|\omega_l|, T) e^{i\omega_l t_j}, \quad (6)$$

where $2M$ is the total number of time steps, $\tau_{\text{sim}}=2M\Delta t$ is the total simulation time, and $\omega_l=2\pi l/\tau_{\text{sim}}$. M_l and N_l are independent Gaussian random numbers with zero mean and a variance of one. Their symmetry properties are $M_l=M_{-l}$ and $N_l=-N_{-l}$. These Gaussian random numbers can be generated by the Marsaglia and Bray modification of the Box-Müller transformation [17], a very fast and reliable method assuming the uniformly distributed random number generator is quick and robust.

The electric field sources generate both electric and magnetic fields, which propagate into the grid. $E(x, \omega)$ and $H(x, \omega)$ are obtained by the discrete Fourier transform (DFT) of $E(x, t)$ and $H(x, t)$. Since both $E(x, t)$ and $H(x, t)$ are real numbers, $E(x, \omega)=E(x, -\omega)$ and $H(x, \omega)=H(x, -\omega)$. The EM energy density at frequency ω shall include $E(x, \omega)$, $E(x, -\omega)$, $H(x, \omega)$, and $H(x, -\omega)$. If the grid is vacuum, the steady-state energy density at every position x should be equal to the blackbody radiation density. The rms amplitude δ of the source field E_s is determined by

$$\frac{1}{2}\epsilon_0|E(x, |\omega|)|^2 + \frac{1}{2}\mu_0|H(x, |\omega|)|^2 = \frac{\hbar}{\pi c} \frac{|\omega|}{e^{\hbar|\omega|/kT} - 1}. \quad (7)$$

When setting the parameters in the FDTD simulation, we must taken into consideration the characteristics of thermal noise. The temporal correlation time or coherence time τ_c of thermal noise is defined as the full width at half maximum (FWHM) of the temporal field correlation function. If the time step Δt is close to τ_c , E_s exhibits a sudden jump at each time step. The 1D FDTD algorithm cannot accurately propagate such steplike pulses (with sharp rising edge) if the Courant factor $S \equiv c\Delta t/\Delta x$ is set at a typical value $S < 1$. The pulse shape is distorted with fringes corresponding to both retarded propagation and superluminal response [1]. This occurs because the higher frequencies from the step discontinuity are being inadequately sampled and because of numerical dispersion arising from the method of obtaining the spatial derivatives for E and H . To avoid such problems, we use $S=1$ which eliminates the numerical dispersion artifact [1]. Furthermore, we set $\Delta t \ll \tau_c$ which provides a dense temporal sampling relative to the correlation and coherence time of the thermal noise.

To obtain an accurate noise spectrum with the DFT, both the frequency and temporal resolutions must be chosen carefully. The two problems affecting the reliability of the DFT are aliasing and leakage due to the use of a finite simulation time [18]. The solution to these problems is to increase the number of time steps $2M$ and decrease the time step value Δt . This takes the DFT closer to a perfect analytical Fourier transform, but run-time and memory limitations must be considered as well. Taking advantage of the FFT algorithm significantly reduces both noise generation time and spectral analysis time.

Although the thermal noise spectrum can be very broad, only noise within a certain frequency range is relevant to a specific problem. Let ω_{min} and ω_{max} denote the lower and upper limits of the frequency range of interest and $\Delta\omega$ denote the frequency resolution needed within this range. To guarantee the accuracy of the noise simulation in $\omega_{\text{min}} < \omega < \omega_{\text{max}}$, the total running time τ_{sim} must exceed $2\pi/\omega_{\text{min}}$ and $2\pi/\Delta\omega$. The time step Δt has an additional requirement, $\Delta t < \pi/\omega_{\text{max}}$.

III. SIMULATION RESULTS

A. Blackbody radiation in vacuum

We first test the noise sources in a 1D FDTD system composed entirely of vacuum. Two sets of independent noise signals $E_s(t_j)$ are generated via Eq. (6). One set is added as a soft source one grid cell away from the left absorbing boundary and the other one cell from the right absorbing boundary. Both have equal rms amplitude δ so that the average EM flux to the left equals that to the right at any position x in the grid. Since the system is one dimensional, the EM flux at any distance away from the source has the same magnitude. The value of δ shall be adjusted so that Eq. (7) is satisfied. For the EM energy density radiated by one source to equal $D(|\omega|, T)$, we set δ to

$$\delta = \sqrt{\frac{2}{\epsilon_0} \frac{1}{6\hbar c}} kT. \quad (8)$$

After the noise fields in the grid reach steady state, the noise spectrum at any grid point is obtained by a DFT. We verify that the spectrum of EM energy density at any point in the grid is identical to that at the source. This means there is no distortion of the noise spectrum by the propagation of noise fields in vacuum. The two point sources at the grid-ABL interface radiate into both the grid and ABL. Since the two sources are uncorrelated with each other, their energy densities, instead of their field amplitudes, add in the grid. Thus no further modification of δ from that given by Eq. (8) is needed to satisfy Eq. (7). It is numerically confirmed that δ does not depend on the total length of the system.

Examples of the noise source of electric field $E_s(t_j)$ at $T = 30\,000$ K and $T = 50\,000$ K are shown in Fig. 1. $\Delta x = 1$ nm and $\Delta t \ll \tau_c$. The frequency range of interest is set as $\omega_{\min} = 2 \times 10^{15}$ Hz, $\omega_{\max} = 2.5 \times 10^{16}$ Hz, and the frequency resolution $\Delta\omega = 1 \times 10^{12}$ Hz. From the condition $\Delta t < \pi/\omega_{\max}$, Δx shall be less than 37 nm. Figure 2 compares the FDTD calculated energy density to that of thermal radiation density $D(\omega, T)$. Using $\Delta x = 10$ nm creates a slight discrepancy at high frequencies; e.g., at $\omega \leq 1 \times 10^{16}$ Hz the mean error $\geq 2.5\%$. To reduce the error to below 2.5% at $\omega_{\max} = 2.5 \times 10^{16}$ Hz, we refine the resolution. Using $\Delta x = 4$ nm changes the error at ω_{\max} to 1.6%. If the total time step $2M = 2^{21}$ is fixed, the decrease of Δt leads to a reduction of $\tau_{\text{sim}} = 2M\Delta t$, which increases $2\pi/\tau_{\text{sim}}$ to 2×10^{11} Hz. We must check that $2\pi/\tau_{\text{sim}} < \omega_{\min}$ and $2\pi/\tau_{\text{sim}} < \Delta\omega$ are still satisfied. With $\Delta x = 1$ nm, the error at 2.5×10^{16} Hz is further reduced to $< 0.1\%$. $2\pi/\tau_{\text{sim}}$ increases to 9×10^{11} Hz, which is still below the set values of ω_{\min} and $\Delta\omega$. Therefore, using the value of δ in Eq. (8) and carefully choosing the numerical resolutions yield the blackbody spectrum at every point in the grid within the frequency range of interest.

Figure 3 compares the FDTD calculated temporal correlation function of the electric field to that of Eq. (4) at $T = 30\,000$ K and $50\,000$ K. With increasing temperature, the coherence time τ_c reduces quickly. The quantitative dependence of τ_c on T is found to be $\tau_c \approx 1.32\hbar/kT$. This $1/T$ dependence does not change for a dimensionality higher than one; only the prefactor changes [19]. As the correlation time τ_c decreases, the time step Δt shall be reduced to maintain the temporal resolution of the correlation function. The subsequent reduction of total running time $\tau_{\text{sim}} = 2M\Delta t$ does not affect the numerical accuracy, as long as the total number of time steps $2M$ is fixed. A decrease of $2M$ would result in an increased mean-square error in the correlation function due to less sampling. As shown in Fig. 3, the good agreement of the FDTD calculated temporal correlation function to that of blackbody radiation given by Eq. (1) confirms that introducing noise sources with the characteristics of blackbody radiation at the FDTD absorbing boundary effectively simulates thermal noise in vacuum.

B. Thermal noise in a 1D cavity

Next we calculate the thermal noise in a dielectric slab of length L and refractive index $n > 1$. This slab constitutes an

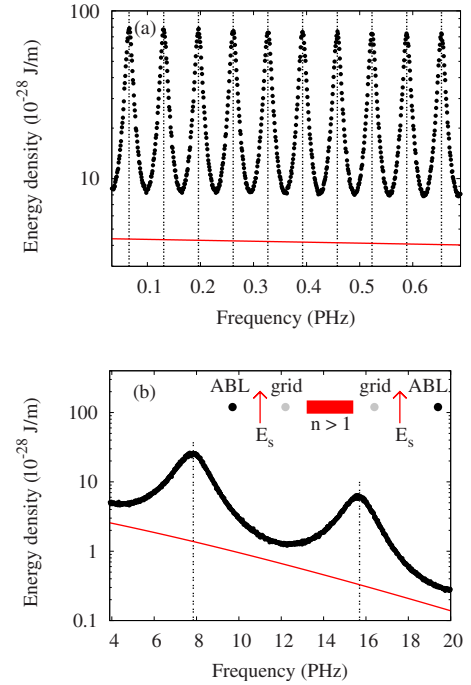


FIG. 4. (Color online) Spatially averaged EM energy density $U(\omega)$, calculated by the FDTD method, vs frequency ω in a dielectric slab cavity with refractive index $n=6$ and length (a) $L = 2400$ nm and (b) $L = 20$ nm. The vertical black dashed lines mark the frequencies of cavity modes ω_m . The spectrum of impinging blackbody radiation $D(\omega, T)$ is also plotted (red solid line). In (a) the cavity decay time $\tau = 143$ ps is much longer than τ_c . In (b), $\tau = 1.19$ fs, comparable to τ_c .

open cavity in that electromagnetic field leakage occurs from both surfaces of the slab into an exterior region. A schematic of the 1D open cavity is shown in the inset of Fig. 4(b). The cavity mode frequency is $\omega_m = m\pi c/nL$, where m is an integer and c is the speed of light in vacuum. The frequency spacing of adjacent modes is $d\omega = \omega_m - \omega_{m-1} = \pi c/nL$, which is independent of m . Ignoring intracavity absorption, the decay of cavity photons is caused only by their escape from the cavity. All the cavity modes have roughly the same decay time $\tau = 1/k_i c$, where $k_i = -\ln(r^2)/2nL$, and $r = (1-n)/(1+n)$ is the reflection coefficient at the boundary of the dielectric slab. The mode linewidth is $\delta\omega = 2/\tau$. We simulate only good cavities whose modes are well separated in frequency, namely $\delta\omega < d\omega$. Since $\delta\omega \propto 1/L$, the ratio $\delta\omega/d\omega$ is independent of L and is only a function of n .

The Langevin equation for the annihilation operator $\hat{a}_m(t)$ of photons in the m th cavity mode is

$$\frac{d\hat{a}_m(t)}{dt} = -\frac{1}{\tau}\hat{a}_m(t) + \hat{F}_m(t), \quad (9)$$

where $\hat{F}_m(t)$ is the Langevin force. If the noise correlation time $\tau_c \ll \tau$, $\hat{F}_m(t)$ can be considered δ -correlated in time. The Markovian approximation gives $\langle \hat{F}_m^\dagger(t) \hat{F}_m(t') \rangle = D_F \delta(t - t')$. According to the fluctuation dissipation theorem, $D_F = (1/\tau)n_T(\omega_m)$, where $n_T(\omega_m) = (e^{\hbar\omega_m/kT} - 1)^{-1}$ is the number

of thermal photons in a vacuum mode of frequency ω_m at temperature T [8].

From Eq. (9), the average photon number in one cavity mode $\langle \hat{n}_m(t) \rangle \equiv \langle \hat{a}_m^\dagger(t) \hat{a}_m(t) \rangle$ satisfies

$$\frac{d}{dt} \langle \hat{n}_m(t) \rangle = -\frac{2}{\tau} \langle \hat{n}_m(t) \rangle + \frac{2}{\tau} n_T(\omega_m). \quad (10)$$

At steady state, $\langle \hat{n}_m \rangle = n_T(\omega_m)$ in each cavity mode. The number of thermal photons is determined by the Bose-Einstein distribution $n_T(\omega_m)$. $\langle \hat{n}_m \rangle$ is independent of the cavity mode decay rate because the amount of thermal fluctuation entering the cavity increases by the same amount as the intracavity energy decay rate.

In our FDTD simulations, we verify that when $\tau \gg \tau_c$ the number of thermal photons in one cavity mode is equal to $n_T(\omega_m)$. Since there is neither a driving field (e.g., a pumping field) nor excited atoms in the cavity, the EM energy stored in one cavity mode comes entirely from the thermal radiation of the ABL which is coupled into that particular mode. The steady-state number of photons in the m th cavity mode is obtained from the FDTD calculation of intracavity EM energy within the frequency range $\omega_{m-1/2} < \omega < \omega_{m+1/2}$, where $\omega_{m \pm 1/2} = (m \pm 1/2) \pi c / nL$,

$$n_m \equiv \langle \hat{n}_m \rangle = \frac{1}{\hbar \omega_m} \int_{\omega_{m-1/2}}^{\omega_{m+1/2}} d\omega \times \int_0^L dx \left(\frac{1}{2} \epsilon |E(x, \omega)|^2 + \frac{1}{2} \mu_0 |H(x, \omega)|^2 \right). \quad (11)$$

In our simulation, the temperature of the thermal sources at the ABL is $T=30\,000$ K. The coherence time of thermal radiation is $\tau_c=0.337$ fs. The refractive index of the dielectric slab is $n=6$ and the length is $L=2400$ nm. The cavity lifetime $\tau=143$ fs is much longer than τ_c . The reason to choose a relatively large value of n is to have $\delta\omega < d\omega$ so that the cavity modes are separated in frequency. Care must be taken in setting the grid resolution because the intracavity wavelength is reduced to λ/n . To maintain the spatial resolution, Δx is decreased to meet $\Delta x \ll \lambda/n$. In our FDTD simulation, $\Delta x=1$ nm and $2M=2^{21}$. After the intracavity EM field reaches the steady state, we calculate the average thermal energy density inside the cavity

$$U(\omega) = \frac{1}{L} \int_0^L dx \left(\frac{1}{2} \epsilon |E(x, \omega)|^2 + \frac{1}{2} \mu_0 |H(x, \omega)|^2 \right). \quad (12)$$

Figure 4(a) shows the intracavity noise spectrum $U(\omega)$, which features peaks at the cavity resonant frequencies ω_m . Because $n > 1$, EM energy is also stored in the dielectric slab at frequencies away from cavity resonances. For example, $U(\omega = \omega_{m \pm 1/2})$ is higher than that in vacuum by a factor of $2n^2/(n^2+1)$. Thus the entire noise spectrum lies on top of the vacuum blackbody radiation spectrum, as confirmed in Fig. 4. The number of thermal photons in a cavity mode is calculated via Eq. (11) and plotted in Fig. 5. The modal photon number n_m is equal to $n_T(\omega_m)$ with a mean error less than 0.1%. This result agrees with the steady-state solution of Eq. (11). It confirms that our numerical model of thermal noise in

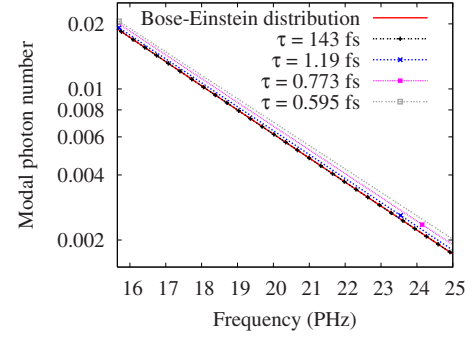


FIG. 5. (Color online) Number of thermal photons in individual cavity modes n_m , calculated via the FDTD method, for a slab cavity with $n=6$. The cavity length L is varied to change τ . The impinging blackbody radiation has $T=30\,000$ K and $\tau_c=0.337$ fs. The values of τ_c/τ are 0.0024, 0.29, 0.43, and 0.56. Lines are drawn to connect the data points at the mode frequencies $\omega_m = \pi cm/nL$ to illustrate their frequency dependence. For $\tau_c \ll \tau$ (only every fifth mode for $\tau=143$ fs is shown to improve the visibility), the photon number n_m coincides with the Bose-Einstein distribution n_T . When $\tau_c \sim \tau$, n_m deviates from n_T .

an open cavity is consistent with the prediction of quantum mechanical theory. Note that the modal photon numbers in Fig. 5 are time averaged values. Their values being much less than unity can be interpreted in a quantum mechanical picture as that most of the time there is no photon in the cavity mode.

The above calculation is done in the Markovian regime. Next we move to the non-Markovian regime by reducing τ . The refractive index is kept at $n=6$, while the cavity length L is reduced. This is a simple way of increasing the mode linewidth $\delta\omega$ while keeping the modes separated in frequency, i.e., keeping $\delta\omega/d\omega$ constant. If τ is decreased to less than τ_c , Δt shall be reduced to keep $\Delta t \ll \tau$. Meanwhile, the increase of the mode linewidth and mode spacing allows low frequency resolution, namely, an increase of $\Delta\omega$. For example, at $L=20$ nm, we set $\Delta x=0.1$ nm, $\Delta\omega=9 \times 10^{12}$ Hz, and $2M=2^{21}$. Figure 4(b) shows the intracavity noise spectrum $U(\omega)$ in this regime, which also features peaks at the cavity resonant frequency ω_m . Figure 5 shows the FDTD-calculated value of n_m as L decreases gradually from 2400 nm to 20 nm. When τ approaches τ_c , n_m is no longer independent of τ , but starts increasing from $n_T(\omega_m)$. This means the number of thermal photons that are captured by a cavity mode increases with the decrease of τ . As the coherence time of thermal radiation impinging onto the cavity approaches the cavity photon lifetime, the constructive interference of the thermal field is improved inside the cavity, leading to a larger buildup of intracavity energy.

We also investigate a different situation where τ is fixed and τ_c is varied. By reducing the temperature T , the coherence time of thermal radiation τ_c is increased. Meanwhile, the energy density of thermal radiation is decreased. As shown in Fig. 6, the number of thermal photons n_m in a cavity mode is reduced. This can be easily understood as there are fewer thermal photons incident onto the cavity at lower T . Nevertheless, n_m is larger than $n_T(\omega_m)$ at the same T . This is because the longer coherence time of the thermal

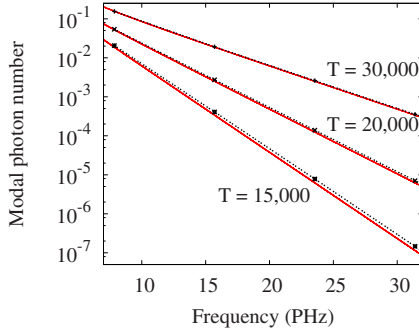


FIG. 6. (Color online) Number of thermal photons in individual cavity modes n_m , calculated via the FDTD method, for a dielectric slab cavity with $n=6$ and $L=20$ nm. The cavity decay time $\tau = 1.19$ fs. The temperature of blackbody radiation is varied to change τ_c . The values of τ_c/τ are 0.29 ($T=30\,000$ K), 0.43 ($T=20\,000$ K), and 0.56 ($T=15\,000$ K). Black dashed lines are drawn to connect the data points at the mode frequencies $\omega_m = \pi cm/nL$ to illustrate their frequency dependence. For comparison, the Bose-Einstein distribution $n_T(\omega)$ is also plotted (red solid lines) for the same temperatures.

field results in better constructive interference inside the cavity.

IV. DISCUSSION

To gain a better understanding of our FDTD simulation results in the non-Markovian regime, we analytically examine the effect of noise correlation time τ_c on the amount of thermal noise inside an open cavity. The ratio of the intracavity EM energy at frequency ω to the energy density of the thermal source outside the cavity is $W(\omega) \equiv \left\{ \int_0^L dx \left[\frac{1}{2} \epsilon |E(x, \omega)|^2 + \frac{1}{2} \mu_0 |H(x, \omega)|^2 \right] \right\} / D(\omega, T)$. For a dielectric slab of refractive index n and length L , we obtain the expression for $W(\omega)$ using the transfer matrix method [20],

$$W(\omega) = \frac{2nc}{\omega} \left[\frac{2\omega nL(1+n^2)/c + (n^2-1)\sin(2\omega nL/c)}{1+6n^2+n^4 - (n^2-1)^2\cos(2\omega nL/c)} \right]. \quad (13)$$

It can be used to calculate the ratio $B_m(\tau_c, \tau) \equiv n_m/n_T(\omega_m)$ as

$$n_m = \left[\int_{\omega_{m-1/2}}^{\omega_{m+1/2}} d\omega W(\omega) D(\omega, T) \right] / \hbar \omega_m. \quad (14)$$

In the Markovian regime $\tau_c \ll \tau$ and $D(\omega, T)$ is nearly constant over the frequency interval of one cavity mode so

$$\begin{aligned} B_m(\tau_c, \tau) &= \frac{D(\omega_m, T)}{\hbar \omega_m n_T(\omega_m)} \int_{\omega_{m-1/2}}^{\omega_{m+1/2}} d\omega W(\omega) \\ &= \frac{1}{\pi c} \int_{\omega_{m-1/2}}^{\omega_{m+1/2}} d\omega W(\omega). \end{aligned} \quad (15)$$

We input the same parameters as the FDTD simulation: $n=6$, $L=2400$ nm, and $\tau=143$ fs. As τ_c approaches zero, the integration of $W(\omega)$ from $\omega_{m-1/2}$ to $\omega_{m+1/2}$ gives a value close to πc . Thus, as shown in the inset of Fig. 7, $B_m(\tau_c, \tau) \approx 1$ for $\tau_c/\tau \ll 1$. The deviation of $B_m(\tau_c, \tau)$ from one is greater for

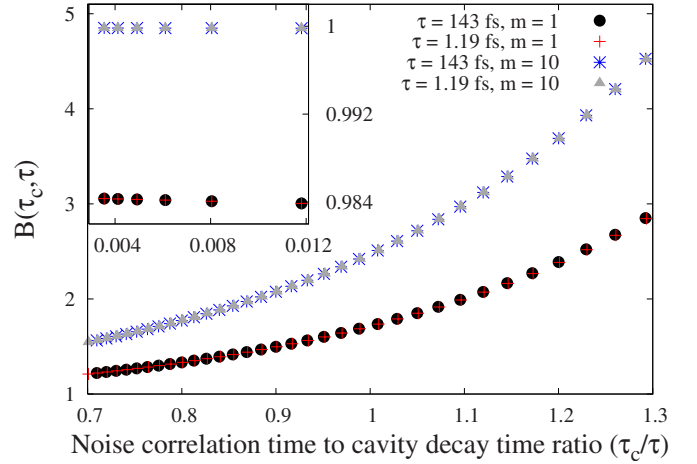


FIG. 7. (Color online) $B_m(\tau_c, \tau) \equiv n_m/n_T(\omega_m)$ vs the ratio of noise correlation time to cavity decay time τ_c/τ . $B_m(\tau_c, \tau)$ depends only on the ratio τ_c/τ and not on τ_c or τ individually. This plot was generated by fixing τ and varying τ_c . Cavity modes of higher m have a larger value of $B_m(\tau_c, \tau)$ whether in the regime $\tau_c \sim \tau$ (main panel) or $\tau_c \ll \tau$ (inset).

smaller m . One possible reason is that the condition $\delta\omega \ll \omega_m$ no longer holds for small m and there is a large uncertainty in defining the frequency of a cavity mode whose linewidth is comparable to its center frequency. In other words, the calculation of n_m using Eq. (14) becomes questionable.

In the non-Markovian regime $\tau_c \gtrsim \tau$, $D(\omega, T)$ is not constant over the frequency range of a cavity mode anymore; thus it cannot be taken out of the integral in Eq. (14). The behavior of $B_m(\tau_c, \tau)$ in this regime is shown in the main panel of Fig. 7. As τ_c approaches τ , $B_m(\tau_c, \tau)$ no longer stays near one but increases with τ_c/τ . This result is consistent with that of the FDTD simulation presented in the previous section. On the one hand, if τ is fixed and τ_c is increased by decreasing the temperature T , the absolute number of thermal photons in a cavity mode n_m decreases, but its ratio to the number of thermal photons in a vacuum mode $n_T(\omega_m)$ increases. On the other hand, if τ_c is fixed and τ is decreased by shortening the cavity length L , both n_m and $n_m/n_T(\omega_m)$ increase. The departure of n_m from $n_T(\omega_m)$ is a direct consequence of the breakdown of the Markovian approximation. When the coherence time of thermal radiation is comparable to the cavity decay time, the Langevin force $\hat{F}_m(t)$ in Eq. (9) is no longer δ -correlated in time and Eq. (10) is invalid.

V. CONCLUSION

We have calculated the fluctuations of EM fields in open cavities due to output coupling with the FDTD method. The fluctuation dissipation theorem dictates that the cavity field dissipation by leakage be accompanied by thermal noise, which is simulated here by classical electrodynamics. The absorbing boundary of the FDTD grid is treated as a blackbody, which radiates into the grid. We have synthesized the noise sources whose spectrum is equal to that of blackbody radiation. Careful selection of numerical parameters in the

FDTD simulation avoids the distortion of the noise spectrum by wave propagation in the 1D grid. It is numerically confirmed that the noise fields propagating in vacuum retain the blackbody spectrum and temporal correlation function. When a cavity is placed in the grid, the thermal radiation is coupled into the cavity and contributes to the thermal noise for the cavity field. We calculate the thermal noise in a 1D dielectric slab cavity. In the Markovian regime where the cavity photon lifetime τ is much longer than the coherence time of thermal radiation τ_c , the FDTD-calculated amount of thermal noise in a cavity mode agrees with that given by the quantum Langevin equation. This validates our numerical model of thermal noise which originates from cavity openness or output coupling. Our FDTD simulation also demonstrates that in the non-Markovian regime the steady-state number of thermal photons in a cavity mode exceeds that in a vacuum mode. This is attributed to the constructive interference of the thermal field inside the cavity.

The advantage of our numerical model is that the thermal noise is added in the time domain without the knowledge of

cavity modes. It can be applied to simulate complex open systems whose modes are not known prior to the FDTD calculations. Our approach is especially useful for very leaky cavities whose modes overlap strongly in frequency, as the thermal noise related to the cavity leakage is introduced naturally without distinguishing the modes. Therefore, we believe the method developed here can be applied to a whole range of quantum optics problems. Although in this paper the FDTD calculation of thermal noise is performed on 1D systems, the extension to 2D and 3D systems is straightforward. We comment that our approach does not apply to the simulation of zero-point fluctuation which has a different physical origin from the thermal noise. However, our numerical method can be used to study the dynamics of EM fields which are excited by arbitrarily correlated noise sources. One potential application is noise radar [21,22]. The propagation, reflection, and scattering of ultrawideband signals utilized by noise radar can be easily simulated using the method developed here.

-
- [1] A. Taflov and S. Hagness, *Computational Electrodynamics* (Artech House, Boston, 2005).
 - [2] J. P. Berenger, *J. Comput. Phys.* **114**, 185 (1994).
 - [3] A. S. Nagra and R. A. York, *IEEE Trans. Antennas Propag.* **46**, 334 (1998).
 - [4] R. W. Ziolkowski, J. M. Arnold, and D. M. Gogny, *Phys. Rev. A* **52**, 3082 (1995).
 - [5] R. W. Ziolkowski, *Appl. Opt.* **36**, 8547 (1997).
 - [6] R. W. Ziolkowski, *IEEE Trans. Antennas Propag.* **45**, 375 (1997).
 - [7] G. M. Slavcheva, J. M. Arnold, and R. W. Ziolkowski, *IEEE J. Sel. Top. Quantum Electron.* **10**, 1052 (2004).
 - [8] H. Haken, *Laser Theory* (Springer, New York, 1983).
 - [9] M. Lax, *Phys. Rev.* **145**, 110 (1966).
 - [10] R. Lang and M. O. Scully, *Opt. Commun.* **9**, 331 (1973).
 - [11] K. Ujihara, *Phys. Rev. A* **16**, 652 (1977).
 - [12] C. Luo, A. Narayanaswamy, G. Chen, and J. D. Joannopoulos, *Phys. Rev. Lett.* **93**, 213905 (2004).
 - [13] D. L. C. Chan, M. Soljačić, and J. D. Joannopoulos, *Phys. Rev. E* **74**, 036615 (2006).
 - [14] A. E. Siegman, *Lasers* (University Science Books, New York, 1986).
 - [15] C. Garrod, *Statistical Mechanics and Thermodynamics* (Oxford University Press, New York, 1995).
 - [16] V. Freilikher, E. Kanziiper, and A. A. Maradudin, *Phys. Rep.* **288**, 127 (1997).
 - [17] M. Brysbaert, *Behav. Res. Methods Instrum. Comput.* **23**, 45 (1991).
 - [18] R. Hamming, *Numerical Methods for Scientists and Engineers* (Dover Publications, Inc., New York, 1986).
 - [19] Y. Kano and E. Wolf, *Proc. Phys. Soc.* **80**, 1273 (1962).
 - [20] M. Born and E. Wolf, *Principles of Optics*, 5th ed. (Pergamon Press, New York, 1975).
 - [21] B. M. Horton, *Proc. IRE* **47**, 821 (1959).
 - [22] I. P. Theron, E. K. Walton, S. Gunawan, and L. Cai, *IEEE Trans. Antennas Propag.* **47**, 1080 (1999).